PERGAMON

International Journal of Solids and Structures 37 (2000) 5629–5652

INTERNATIONAL JOURNAL OF SOLIDS and STRUCTURES

www.elsevier.com/locate/ijsolstr

Solution of inverse problems by boundary integral equations without residual minimization

Rafael Gallego*, Javier Suárez

Department of Structural Mechanics, Universidad de Granada, Colegio Máximo de Cartuja, 18071 Granada, Spain

Received 28 October 1998; in revised form 25 September 1999

Abstract

In this paper the solution of some inverse problems for potential fields is tackled. The aim is to compute the position and shape of an unknown flaw within a body, using some experimental measures as additional data. By the linearization of the difference between the Boundary Integral Equation for the actual configuration and the same equation for an assumed configuration, an integral equation for the variations is deduced. This integral equation is carried to the boundary by a limiting process and a solution procedure is devised to compute an approximation to the actual flaw. The solution method proceeds iteratively, solving a direct and an inverse problem in every step, but no minimization algorithm is involved. The performance of the method is shown in several numerical examples. © 2000 Elsevier Science Ltd. All rights reserved.

Keywords: Inverse problems; Identification problems; Sensitivity calculation; Boundary element method; Hypersingular kernels

1. Introduction

The present paper deals with the solution of some ill-posed problems which arise in several innovative nondestructive techniques for testing materials and other fields in engineering. The experimental procedures provide, in some cases, only qualitative information about defects or flaws inside the material, but not quantitative results. To complete this information, several computational techniques have been devised, based on finite differences, finite elements, and, more recently, boundary elements. All these techniques try to solve an *inverse problem*, i.e., a problem where some information needed for the direct solution of the problem is lacking, and it has to be computed using some measured data as additional information.

* Corresponding author. Fax: +349-58-248955.
E-mail address: gallego@goliat.ugr.es (R. Gallego).

0020-7683/00/$ - see front matter © 2000 Elsevier Science Ltd. All rights reserved.
PII: S0020-7683(99)00291-7

The boundary element method is a very apt tool for solving a large class of inverse problems where the unknown is the boundary or part of it (a flaw) since it reduces the modeling effort to a minimum. These problems have been tackled by several researchers by the boundary element method and different approaches have been proposed. Tanaka and Masuda (1989) used Taylor expansions with respect to the design variables of the kernels and densities to obtain an integral equation for the sensitivities. They solved the resulting integral equation iteratively but obtained good convergence only with many experimental measurements (52 and more) and if the assumed flaw was close to the real one. The reason may be that they disregarded the variation of the variables with respect to the change of the geometry, obtaining, therefore, an incomplete integral equation. Nishimura and Kobayashi (1991) tackled the identification of cracks using the flux Boundary Integral Equation (BIE) for the direct problem and the potential BIE to define a cost functional. They obtained good results, although a serious shortcoming of their approach is that both potential and flux have to be known along all the exterior boundary. Mitra and Das (1992) solved the identification inverse problem for the Laplace equation minimizing a functional that did not contain any integration along the boundary of the flaw. However, they computed the sensitivities of the functional by finite differences, therefore obtaining a slow convergence. Zeng and Saigal (1992) developed a formulation for potential fields based on variations. Their approach was similar to the Taylor expansion method proposed by Tanaka and Masuda (1989) although more rigorous, but it was not completed either, as it will be shown in this paper. In addition, the authors neither wrote their integral equation for a boundary point nor numerically solved the equation. Mellings and Aliabadi (1993) developed a procedure for the identification of cracks in two-dimensional potential problems. They used implicit differentiation to compute the sensitivities and the BFGS algorithms to minimize a quadratic residual. Nishimura and Kobayashi (1994) extended the ideas of their aforementioned paper and were able to increase the number of design variables using regularization techniques. Bonnet (1995) proposed the material differentiation approach in order to compute the sensitivities of the cost functional. He applied this technique to the detection of obstacles in three-dimensional linear acoustic media and obtained very good convergence for infinite bodies. Finally, Nishimura (1997) describes recent developments in the inverse Boundary Element Method for crack determination. He presented results for both potential problems and elastodynamics. A recent and complete introduction to the topic of inverse problems in Solid Mechanics can be found in the book by Bui (1994).

In this paper, the *identification* of a flaw whose shape and position is unknown beforehand is tackled, although the equations are valid for the *reconstruction* problem as well, where the geometry is known but the boundary conditions are not completely specified. Only the case of cavities excited by a potential field (thermal, antiplane elasticity, ...) is considered but the extension of this procedure to cracks, inhomogeneities, and other excitation fields (acoustic, elastic, elastodynamics, ...) fields, is straightforward and is under way. The problem is the following: for a given body with an unknown interior cavity, an excitation is applied on its boundary and the response is measured at some points on the boundary; the aim is to find the shape and position of the unknown cavity using the additional data provided by the experimental measurements.

Most of the papers which deal with this problem propose solution procedures based on optimization algorithms such as conjugate gradients, BFGS, etc. An objective function or residual is defined as the difference between the computed variables and the measured ones, and the algorithm seeks the shape/position of the flaw such that the objective function attains a minimum.

In this work, we propose a different approach which is based on a Boundary Integral Equation for the *variation* of the potential and flux. These variations are defined as the difference between a measured quantity and its computed value for an assumed flaw. The *Variation Boundary Integral Equation* involves as unknowns the variation of the potential and flux in part of the boundary and the *variation of the geometry*, which are computed from the known boundary conditions for the variations and the

experimental data. The Variation Boundary Integral Equation is discretized using advanced Boundary Elements (BEs) (hypersingular kernels are involved), and the ensuing algebraic system of equations is solved by least squares, since the number of unknowns is less than the number of equations. Some numerical examples are presented, which assess the performance of the proposed procedure.

2. Inverse problems for potential fields

For a given *direct* or *primary* problem, different *inverse* problems can be consider. In all cases, part of the data which is known for a well-posed direct problem is not known. In order to find this unknown data, supplementary information have to be provided. Therefore, many different inverse problems can be posed, although only some of them may be of interest in practical applications. In this section, the problem statement for the so-called identification and reconstruction cases is presented, although only the first and more difficult one is going to be detailed in the sequel.

2.1. Direct problem statement

The *direct* problem is very well known and can be stated as follows:

$$\nabla^2 u(\mathbf{x}) + \psi(\mathbf{x}) = 0; \quad \mathbf{x} \in \Omega \tag{1}$$

with essential and/or natural boundary conditions,

$$u(\mathbf{x}) = \bar{u}; \quad \mathbf{x} \in \Gamma_u$$

$$q(\mathbf{x}) = \bar{q}; \quad \mathbf{x} \in \Gamma_q$$

where $u(\mathbf{x})$ is the potential at a point $\mathbf{x}$ of the domain Ω; $q(\mathbf{x}) = \partial u/\partial \mathbf{n}$ is the flux at a point $\mathbf{x}$ on the boundary Γ whose outward normal is $\mathbf{n}(\mathbf{x})$; $\psi(\mathbf{x})$ is a given source function: in the sequel $\psi(\mathbf{x}) = 0$ is considered, without lost of generality. Finally, $\bar{u}$ and $\bar{q}$ represent known values of the potential and flux on Γ_u and Γ_q, respectively, where $\Gamma_u \cup \Gamma_q = \Gamma$ and $\Gamma_u \cap \Gamma_q = \varnothing$

2.2. Identification inverse problem

In the identification problem, a portion of the boundary, termed, Γ_h, is not known. Usually, Γ_h represents the boundary of an interior flaw whose shape and location is sought. In order to find this flaw, additional data has to be provided, besides the known boundary conditions. For example, experimental measurements may be available at a set of points on Γ_c, the known portion of the boundary,

$$u(\mathbf{x}_\alpha) = \bar{u}(\mathbf{x}_\alpha), \quad \mathbf{x}_\alpha \in \Gamma_c$$

$$q(\mathbf{x}_\beta) = \bar{q}(\mathbf{x}_\beta), \quad \mathbf{x}_\beta \in \Gamma_c$$

where $\alpha = 1, \ldots, M_u$ and, $\beta = 1, \ldots, M_q$ and therefore, $M = M_u + M_q$ supplementary values are known. In addition, measurements at points inside the domain Ω can be provided as well.

2.3. Reconstruction inverse problem

In the reconstruction inverse problem, the geometry of the problem is determined, but the boundary conditions are not completely known. This problem arises in cases where a portion of the boundary is exposed to environmental conditions which can not be assessed due to physical difficulties or geometrical inaccessibility. The aim in the reconstruction inverse problem is to find the unknown boundary conditions based on the supplementary data provided on the boundary and/or the domain, as in the identification problem. Obviously, an inverse problem can be defined where both reconstruction of boundary conditions and identification of part of the boundary were necessary.

2.4. Boundary integral equation for the potential problem

In the identification problem, the boundary Γ_h is the main unknown of the problem. Therefore, the statement of the problems in terms of BIEs appears as the very promising approach.

The potential problem stated in differential form in Eq. (1) can be written in terms of BIE (Brebbia and Dominguez, 1978) by the equation,

$$c(\mathbf{x})u(\mathbf{x}) = \int_{\Gamma} \left[u^*(\mathbf{y};\mathbf{x})q(\mathbf{y}) - q^*(\mathbf{y};\mathbf{x})u(\mathbf{y})\right] \mathrm{d}\Gamma(\mathbf{y}) \tag{2}$$

where $c(\mathbf{x})$, called the free term, is 0 if $\mathbf{x} \notin \Omega \cup \Gamma$, 1 if $\mathbf{x} \in \Omega$ and $\theta/2\pi$ if $\mathbf{x} \in \Gamma$, where θ is the interior angle between the left and right tangents to the boundary at the point $\mathbf{x}$; $u^*(\mathbf{y};\mathbf{x}) = (1/2\pi)\ln(1/r)$ is the *fundamental solution* for the Laplace equation; $r = |\mathbf{y} - \mathbf{x}|$ is the distance between the *collocation* point $\mathbf{x}$ and the *integration* or *observation* point $\mathbf{y}$; and $q^*(\mathbf{y};\mathbf{x}) = -(1/2\pi r)(\partial r/\partial \mathbf{n})$ is the flux associated to the potential $u^*(\mathbf{y};\mathbf{x})$.

3. Variation of the boundary integral equation

Consider a problem where a real flaw has the (unknown) boundary $\tilde{\Gamma}_h$. The value of the potential at any point $\mathbf{x}$ is $u(\mathbf{x}, \tilde{\Gamma}_h)$, where the new parameter $\tilde{\Gamma}_h$ emphasizes that the potential depends on the location of the flaw. Likewise the flux is called $q(\mathbf{x}, \tilde{\Gamma}_h)$. For an assumed location of the flaw, say Γ_h, the potential and the flux are $u(\mathbf{x}, \Gamma_h)$ and $q(\mathbf{x}, \Gamma_h)$, respectively.

The actual domain is called $\tilde{\Omega}$ in the sequel, while the assumed domain, that is, the domain with the assumed flaw is called Ω. To convert the assumed domain Ω to the actual domain $\tilde{\Omega}$, a point $\mathbf{x}$ is applied to a new point $\tilde{\mathbf{x}} = \mathbf{x} + \delta\mathbf{x}$, where $\delta\mathbf{x}$ is the *variation of the geometry*. It has to be emphasized that the whole domain is distorted in order to change the shape and position of the flaw from its assumed location to the actual one (Fig. 1), and not only the points on the boundary of the flaw. Previous works (Zeng and Saigal, 1992) disregarded this fact which is very important in order to arrive at the right BIE.

Eq. (2) can be written for an interior point $\mathbf{x}$ in the assumed domain,

$$\begin{aligned} u(\mathbf{x}, \Gamma_h) = & \int_{\Gamma_c} \left[u^*(\mathbf{y};\mathbf{x})q(\mathbf{y}, \Gamma_h) - q^*(\mathbf{y};\mathbf{x})u(\mathbf{y}, \Gamma_h)\right] \mathrm{d}\Gamma(\mathbf{y}) \\ & + \int_{\Gamma_h} \left[u^*(\mathbf{y};\mathbf{x})q(\mathbf{y}, \Gamma_h) - q^*(\mathbf{y};\mathbf{x})u(\mathbf{y}, \Gamma_h)\right] \mathrm{d}\Gamma(\mathbf{y}) \end{aligned} \tag{3}$$

and the same equation can be set at the corresponding point $\tilde{\mathbf{x}}$ in the actual domain,

$$u(\tilde{\mathbf{x}}, \tilde{\Gamma}_h) = \int_{\Gamma_c} \left[u^*(\mathbf{y}; \tilde{\mathbf{x}}) q(\mathbf{y}, \tilde{\Gamma}_h) - q^*(\mathbf{y}; \tilde{\mathbf{x}}) u(\mathbf{y}, \tilde{\Gamma}_h)\right] \mathrm{d}\Gamma(\mathbf{y}) + \int_{\tilde{\Gamma}_h} \left[u^*(\tilde{\mathbf{y}}; \tilde{\mathbf{x}}) q(\tilde{\mathbf{y}}, \tilde{\Gamma}_h) - q^*(\tilde{\mathbf{y}}; \tilde{\mathbf{x}}) u(\tilde{\mathbf{y}}, \tilde{\Gamma}_h)\right] \mathrm{d}\Gamma(\tilde{\mathbf{y}}) \tag{4}$$

To derive the variation of the integral equation (Eq. (2)) the difference of Eqs. (3) and (4) will be computed and linearized with respect to the variation of the geometry $\delta\mathbf{x}$.

3.1. Variation of the potential and the flux

The linearized integral equation will be written in terms of the difference of the potential and flux between the actual and the assumed domain. Then, the variation of the potential in the assumed configuration is defined as:

$$\delta u(\mathbf{x}) = u(\mathbf{x}, \tilde{\Gamma}_h) - u(\mathbf{x}, \Gamma_h) \tag{5}$$

Therefore, δu represents the difference in the potential *at a given point* $\mathbf{x}$ due to the variation of the boundary of the domain. To define δq, extra care has to be exercised since the flux is defined at the boundary of the domain, and this boundary changes when the geometry is distorted. Taking into account that $q(\mathbf{x}) = \partial u/\partial \mathbf{n} = \nabla u(\mathbf{x}) \cdot \mathbf{n}(\mathbf{x})$, the following definition has been adopted in this paper,

$$\delta q(\mathbf{x}) = \left[\nabla u(\mathbf{x}, \tilde{\Gamma}_h) - \nabla u(\mathbf{x}, \Gamma_h)\right] \cdot \mathbf{n}(\mathbf{x}) = \nabla \delta u(\mathbf{x}) \cdot \mathbf{n}(\mathbf{x}) \tag{6}$$

There are different alternatives to define the variation of the flux, as will be shown when dealing with the series expansion of the variables.

3.2. Variation integral equation

To derive the Variation Integral Equation, the variables at the actual configuration are written in terms of their values at the assumed configuration, their gradients and the variation of the potential, the flux and the geometry, as it is shown in the sequel.

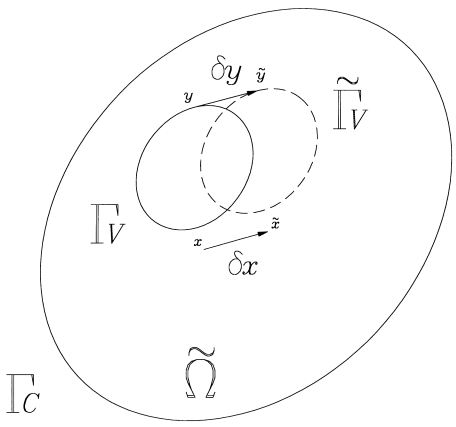

Fig. 1. Change of the domain from the assumed configuration to the actual one.

First of all,

$$u\left(\tilde{\mathbf{x}}, \tilde{\Gamma}_h\right) = u(\mathbf{x}, \Gamma_h) + \delta u(\mathbf{x}) + \nabla u(\mathbf{x}, \Gamma_h) \cdot \delta\mathbf{x} + \text{h.o.t.} \tag{7}$$

to linear order, since $\delta u(\mathbf{x})$ stands for the difference due to the variation of the boundary of the domain, and $\nabla u(\mathbf{x}, \Gamma_h) \cdot \delta\mathbf{x}$ is the term due to the difference between $\tilde{\mathbf{x}}$ and $\mathbf{x}$. Therefore, when computing the difference between Eqs. (4) and (3), on the left-hand side, we obtain,

$$u\left(\tilde{\mathbf{x}}, \tilde{\Gamma}_h\right) - u(\mathbf{x}, \Gamma_h) \simeq \delta u(\mathbf{x}) + \nabla u(\mathbf{x}, \Gamma_h) \cdot \delta\mathbf{x} \tag{8}$$

neglecting the higher order terms.

On the right-hand side, we find several differences of integrals which we will handle separately. Consider first,

$$\delta I_1 = \int_{\Gamma_c} u^*(\mathbf{y}; \tilde{\mathbf{x}}) q\left(\mathbf{y}, \tilde{\Gamma}_h\right) \mathrm{d}\Gamma(\mathbf{y}) - \int_{\Gamma_c} u^*(\mathbf{y}; \mathbf{x}) q(\mathbf{y}, \Gamma_h) \, \mathrm{d}\Gamma(\mathbf{y}) \tag{9}$$

The kernel $u^*(\mathbf{y}; \tilde{\mathbf{x}})$ can be expanded as,

$$u^*(\mathbf{y}; \tilde{\mathbf{x}}) = u^*(\mathbf{y}; \mathbf{x}) + \nabla_x u^*(\mathbf{y}; \mathbf{x}) \cdot \delta\mathbf{x} + \text{h.o.t.} \tag{10}$$

where the subscripts in ∇_{x} means differentiation with respect to the collocation point $\mathbf{x}$. However, u^* is a function on $|\mathbf{y} - \mathbf{x}|$ and, therefore, $\nabla_{\mathrm{x}} u^*(\mathbf{y}; \mathbf{x}) = -\nabla_{\mathrm{y}} u^*(\mathbf{y}; \mathbf{x})$.

Then,

$$u^*(\mathbf{y}; \tilde{\mathbf{x}}) = u^*(\mathbf{y}; \mathbf{x}) - \nabla u^*(\mathbf{y}; \mathbf{x}) \cdot \delta\mathbf{x} + \text{h.o.t.} \tag{11}$$

where the subscript $\mathbf{y}$ will be dropped in the sequel.

The flux, given by $q(\mathbf{y}, \tilde{\Gamma}_h) = \nabla u(\mathbf{y}, \tilde{\Gamma}_h) \cdot \mathbf{n}(\mathbf{y})$, can be expanded as,

$$q\left(\mathbf{y}, \tilde{\Gamma}_h\right) = \nabla\left[u(\mathbf{y}, \Gamma_h) + \delta u(\mathbf{y})\right] \cdot \mathbf{n}(\mathbf{y}) + \text{h.o.t.} \tag{12}$$

using the definition of δu in Eq. (5). Taking into account Eq. (6), the expansion

$$q\left(\mathbf{y}, \tilde{\Gamma}_h\right) = q(\mathbf{y}, \Gamma_h) + \delta q(\mathbf{y}) + \text{h.o.t.} \tag{13}$$

is finally obtained.

Substituting Eqs. (11) and (13) in Eq. (9) and neglecting higher order terms, we obtain,

$$\delta I_1 \simeq \int_{\Gamma_c} \left[u^*(\mathbf{y}; \mathbf{x}) \delta q(\mathbf{y}) - \nabla u^*(\mathbf{y}; \mathbf{x}) q(\mathbf{y}, \Gamma_h) \cdot \delta\mathbf{x}\right] \mathrm{d}\Gamma(\mathbf{y}) \tag{14}$$

Now consider the difference,

$$\delta I_2 = \int_{\Gamma_c} q^*(\mathbf{y}; \tilde{\mathbf{x}}) u\left(\mathbf{y}, \tilde{\Gamma}_h\right) \mathrm{d}\Gamma(\mathbf{y}) - \int_{\Gamma_c} q^*(\mathbf{y}; \mathbf{x}) u(\mathbf{y}, \Gamma_h) \, \mathrm{d}\Gamma(\mathbf{y}) \tag{15}$$

The kernel $q^*(\mathbf{y}; \tilde{\mathbf{x}}) = \nabla_{\mathrm{y}} u^*(\mathbf{y}; \tilde{\mathbf{x}}) \cdot \mathbf{n}(\mathbf{y})$ is expanded as,

$$q^*(\mathbf{y}; \tilde{\mathbf{x}}) = \nabla_{\mathrm{y}} u^*(\mathbf{y}; \tilde{\mathbf{x}}) \cdot \mathbf{n}(\mathbf{y}) + \nabla_{\mathrm{x}}\left[\nabla_{\mathrm{y}} u^*(\mathbf{y}; \mathbf{x}) \cdot \mathbf{n}(\mathbf{y})\right] \cdot \delta\mathbf{x} + \text{h.o.t.} \tag{16}$$

or

$$q^*(\mathbf{y};\tilde{\mathbf{x}}) = q^*(\mathbf{y};\mathbf{x}) - \nabla q^*(\mathbf{y};\mathbf{x})\cdot\delta\mathbf{x} + \text{h.o.t.} \tag{17}$$

where $\nabla q^*(\mathbf{y};\mathbf{x})$ is a short form of $\nabla[\nabla u^*(\mathbf{y};\mathbf{x})]\cdot\mathbf{n}(\mathbf{y})$.

Substituting this equation and the expansion of $u(\mathbf{y},\tilde{\Gamma}_h)$ given by Eq. (7) in Eq. (15), and neglecting second-order terms, we obtain,

$$\delta I_2 \simeq \int_{\Gamma_c}\left[q^*(\mathbf{y};\mathbf{x})\delta u(\mathbf{y}) - \nabla q^*(\mathbf{y};\mathbf{x})u(\mathbf{y},\Gamma_h)\cdot\delta\mathbf{x}\right]\mathrm{d}\Gamma(\mathbf{y}) \tag{18}$$

Third, consider,

$$\delta I_3 = \int_{\tilde{\Gamma}_h} u^*(\tilde{\mathbf{y}};\tilde{\mathbf{x}})q\big(\tilde{\mathbf{y}},\tilde{\Gamma}_h\big)\,\mathrm{d}\Gamma(\tilde{\mathbf{y}}) - \int_{\Gamma_h} u^*(\mathbf{y};\mathbf{x})q(\mathbf{y},\Gamma_h)\,\mathrm{d}\Gamma(\mathbf{y}) \tag{19}$$

In order to perform both integrals in this expression along the assumed boundary Γ_h, we can write,

$$\mathrm{d}\Gamma(\tilde{\mathbf{y}}) = (1+\delta J)\,\mathrm{d}\Gamma(\mathbf{y}) \tag{20}$$

Taking into account that $\mathrm{d}\Gamma(\mathbf{y}) = |\mathrm{d}\mathbf{y}| = (\mathrm{d}\mathbf{y}\cdot\mathrm{d}\mathbf{y})^{1/2}$ and, $\mathrm{d}\Gamma(\tilde{\mathbf{y}}) = |\mathrm{d}\mathbf{y}+\delta\mathrm{d}\mathbf{y}| = [(\mathrm{d}\mathbf{y}+\delta\mathrm{d}\mathbf{y})\cdot(\mathrm{d}\mathbf{y}+\delta\mathrm{d}\mathbf{y})]^{1/2}$, (see Fig. 2), and clearing δJ from the former equation, one can write,

$$\delta J = \frac{\mathrm{d}\Gamma(\tilde{\mathbf{y}})}{\mathrm{d}\Gamma(\mathbf{y})} - 1 = \frac{\left[(\mathrm{d}\mathbf{y}+\delta\mathrm{d}\mathbf{y})\cdot(\mathrm{d}\mathbf{y}+\delta\mathrm{d}\mathbf{y})\right]^{1/2}}{(\mathrm{d}\mathbf{y}\cdot\mathrm{d}\mathbf{y})^{1/2}} - 1 \tag{21}$$

Expanding the dot product in the numerator and neglecting higher order terms, one gets,

$$\delta J = \left(1 + 2\frac{\mathrm{d}\mathbf{y}\cdot\delta\mathrm{d}\mathbf{y}}{\mathrm{d}\mathbf{y}\cdot\mathrm{d}\mathbf{y}}\right)^{1/2} - 1 \tag{22}$$

Finally, taking into account $(1+x)^{1/2} = 1 + (1/2)x + \text{h.o.t.}$ for $x \ll 1$, the expansion,

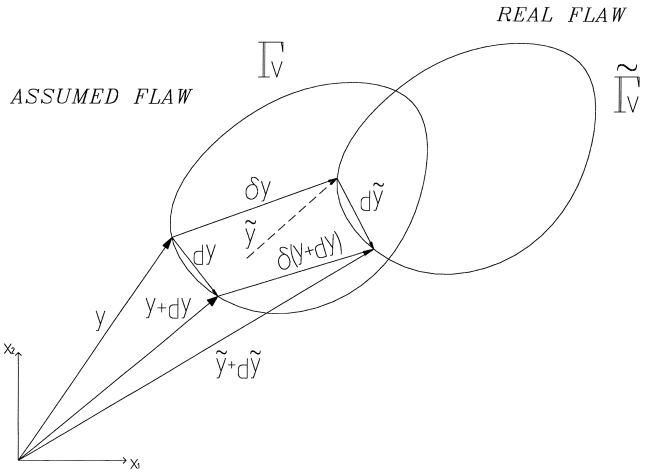

Fig. 2. Distortion of the boundary of the flaw.

$$\delta J = \frac{\mathrm{d}\mathbf{y} \cdot \delta \mathrm{d}\mathbf{y}}{\mathrm{d}\mathbf{y} \cdot \mathrm{d}\mathbf{y}} + \text{h.o.t.} \tag{23}$$

is obtained.

Then, δI_3 can be written as,

$$\delta I_3 \simeq \int_{\Gamma_h} \left[u^*(\tilde{\mathbf{y}}; \tilde{\mathbf{x}}) q\big(\tilde{\mathbf{y}}, \tilde{\Gamma}_h\big)(1 + \delta J) - u^*(\mathbf{y}; \mathbf{x}) q(\mathbf{y}, \Gamma_h) \right] \mathrm{d}\Gamma(\mathbf{y}) \tag{24}$$

Now, the kernel $u^*(\tilde{\mathbf{y}}; \tilde{\mathbf{x}})$ has to be expanded both in $\mathbf{x}$ and $\mathbf{y}$. Therefore,

$$u^*(\tilde{\mathbf{y}}; \tilde{\mathbf{x}}) = u^*(\mathbf{y}; \mathbf{x}) + \nabla_{\mathrm{x}} u^*(\mathbf{y}; \mathbf{x}) \cdot \delta\mathbf{x} + \nabla_{\mathrm{y}} u^*(\mathbf{y}; \mathbf{x}) \cdot \delta\mathbf{y} + \text{h.o.t.} \tag{25}$$

or,

$$u^*(\tilde{\mathbf{y}}; \tilde{\mathbf{x}}) = u^*(\mathbf{y}; \mathbf{x}) + \nabla u^*(\mathbf{y}; \mathbf{x}) \cdot (\delta\mathbf{y} - \delta\mathbf{x}) + \text{h.o.t.} \tag{26}$$

On the other hand, for the expansion of the flux, both the variation of the calculation point and the variation of the outward normal have to taken into account.Therefore,

$$q\big(\tilde{\mathbf{y}}, \tilde{\mathbf{\Gamma}}_h\big) = \big[\nabla u(\mathbf{y}, \Gamma_h) + \nabla \delta u(\mathbf{y}) + \nabla\big[\nabla u(\mathbf{y}, \Gamma_h)\big] \cdot \delta\mathbf{y}\big] \cdot \big[\mathbf{n}(\mathbf{y}) + \delta\mathbf{n}(\mathbf{y})\big] + \text{h.o.t.} \tag{27}$$

Expanding the dot product, neglecting second-order terms and taking into account the definition of the flux variation in Eq. (6), we obtain,

$$q\big(\tilde{\mathbf{y}}, \tilde{\Gamma}_h\big) \simeq q(\mathbf{y}, \Gamma_h) + \delta q(\mathbf{y}) + \nabla u(\mathbf{y}, \Gamma_h) \cdot \delta\mathbf{n}(\mathbf{y}) + \nabla q(\mathbf{y}, \Gamma_h) \cdot \delta\mathbf{y} \tag{28}$$

where $\nabla q(\mathbf{y}, \Gamma_h)$ is a short form of $\nabla[\nabla u(\mathbf{y}, \Gamma_h)] \cdot \mathbf{n}(\mathbf{y})$.

In regard to the variation of the outward normal, it can be readily shown that,

$$\delta\mathbf{n} = \delta\mathbf{m} - \mathbf{n}\delta J \tag{29}$$

where $\delta\mathbf{m} = (\nabla y_2 \cdot \mathbf{t}, -\nabla y_1 \cdot \mathbf{t})$; $\mathbf{t}$ is the tangent vector to the boundary.

If Eqs. (26), (28) and (29) are substituted in Eq. (24), and second-order terms are neglected, the following expansion is obtained,

$$\begin{aligned} \delta I_3 \simeq \int_{\Gamma_h} \big[& u^*(\mathbf{y}; \mathbf{x}) \delta q(\mathbf{y}) + u^*(\mathbf{y}; \mathbf{x}) \nabla u(\mathbf{y}, \Gamma_h) \cdot \delta\mathbf{m}(\mathbf{y}) + u^*(\mathbf{y}; \mathbf{x}) \nabla q(\mathbf{y}, \Gamma_h) \cdot \delta\mathbf{y} + \nabla u^*(\mathbf{y}; \mathbf{x}) q(\mathbf{y}, \Gamma_h) \\ & \cdot (\delta\mathbf{y} - \delta\mathbf{x}) \big] \mathrm{d}\Gamma(\mathbf{y}) \end{aligned} \tag{30}$$

Finally, a similar approach can be used to linearized the fourth and last expression,

$$\delta I_4 = \int_{\tilde{\Gamma}_h} q^*(\tilde{\mathbf{y}}; \tilde{\mathbf{x}}) u\big(\tilde{\mathbf{y}}, \tilde{\Gamma}_h\big) \, \mathrm{d}\Gamma(\tilde{\mathbf{y}}) - \int_{\Gamma_h} q^*(\mathbf{y}; \mathbf{x}) u(\mathbf{y}, \Gamma_h) \, \mathrm{d}\Gamma(\mathbf{y}) \tag{31}$$

the result being,

$$\delta I_4 \simeq \int_{\Gamma_h} \left[q^*(\mathbf{y};\mathbf{x})\delta u(\mathbf{y},\Gamma_h) + \nabla u^*(\mathbf{y};\mathbf{x}) u(\mathbf{y},\Gamma_h)\cdot\delta\mathbf{m}(\mathbf{y}) + q^*(\mathbf{y};\mathbf{x})\nabla u(\mathbf{y},\Gamma_h)\cdot\delta\mathbf{y} + \nabla q^*(\mathbf{y};\mathbf{x}) u(\mathbf{y},\Gamma_h)\cdot(\delta\mathbf{y}-\delta\mathbf{x})\right] \mathrm{d}\Gamma(\mathbf{y}) \tag{32}$$

where, again, $\nabla q^* = \nabla[\nabla u^*(\mathbf{y};\mathbf{x})]\cdot\mathbf{n}(\mathbf{y})$.

Collecting the variations given by Eqs. (8), (14), (18), (30) and (32), the following *Variation Boundary Integral Equation* is obtained,

$$\begin{aligned}\delta u(\mathbf{x}) + \nabla u(\mathbf{x},\Gamma_h)\cdot\delta\mathbf{x} = & \int_{\Gamma}\left[u^*(\mathbf{y};\mathbf{x})\delta q(\mathbf{y}) - q^*(\mathbf{y};\mathbf{x})\delta u(\mathbf{y})\right]\mathrm{d}\Gamma(\mathbf{y}) \\ & - \int_{\Gamma_c}\left[\nabla u^*(\mathbf{y};\mathbf{x}) q(\mathbf{y},\Gamma_h) - \nabla q^*(\mathbf{y};\mathbf{x}) u(\mathbf{y},\Gamma_h)\right]\cdot\delta\mathbf{x}\, d\Gamma(y) \\ & + \int_{\Gamma_h}\left[\left[\nabla u^*(\mathbf{y};\mathbf{x}) q(\mathbf{y},\Gamma_h) - \nabla q^*(\mathbf{y};\mathbf{x}) u(\mathbf{y},\Gamma_h)\right]\cdot(\delta\mathbf{y}-\delta\mathbf{x})\right. \\ & + \left[u^*(\mathbf{y};\mathbf{x})\nabla q(\mathbf{y},\Gamma_h) - q^*(\mathbf{y};\mathbf{x})\nabla u(\mathbf{y},\Gamma_h)\right]\cdot\delta\mathbf{y} \\ & \left. + \left[u(\mathbf{y};\mathbf{x})\nabla u(\mathbf{y},\Gamma_h) - \nabla u^*(\mathbf{y};\mathbf{x}) u(\mathbf{y},\Gamma_h)\right]\cdot\delta\mathbf{m}(\mathbf{y})\right]\mathrm{d}\Gamma(\mathbf{y})\end{aligned} \tag{33}$$

The former equation relates the variation of the potential and the geometry at a point $\mathbf{x}\in\Omega$, with the variation of the potential, flux and geometry along the boundary of the domain. The potential and flux of the primary problem on the assumed configuration and their gradients appear in the equation as well, but both can be computed by solving the direct problem.

This integral equation would be much more useful if we are able to write it for a point $\boldsymbol{\xi}\in\Gamma$, since, in such case, only quantities along the boundary will be involved. A careful limiting process is performed in the next section to carry $\mathbf{x}\to\boldsymbol{\xi}\in\Gamma$

4. Variation boundary integral equation for a point on the boundary

In order to obtain the sought after Variation Boundary Integral Equation, a careful limiting process as the one performed for other formulations is carried out (see Guiggiani, 1992 and Gallego and Domínguez, 1996)

To perform the limit of Eq. (33) as $\mathbf{x}\to\boldsymbol{\xi}\in\Gamma$ two cases will be considered: $\boldsymbol{\xi}\in\Gamma_c$ and $\boldsymbol{\xi}\in\Gamma_h$.

The first case is readily carried out since $\delta\mathbf{x}=0$, and therefore, the singularities involved are those of u^* and q^*, as in the direct BIE given in Eq. (2). Thus, when $\mathbf{x}\to\boldsymbol{\xi}\in\Gamma_c$, Eq. (33) leads to,

$$\begin{aligned}c(\boldsymbol{\xi})\delta u(\boldsymbol{\xi}) = & \int_{\Gamma}\left(u^*\delta q - q^*\delta u\right)\mathrm{d}\Gamma + \int_{\Gamma_h}\left[\left(\nabla u^* q - \nabla q^* u\right)\cdot\delta\mathbf{y}\right. \\ & \left. + \left(u^*\nabla q - q^*\nabla u\right)\cdot\delta\mathbf{y} + \left(u^*\nabla u - \nabla u^* u\right)\cdot\delta\mathbf{m}\right]\mathrm{d}\Gamma\end{aligned} \tag{34}$$

where $c(\boldsymbol{\xi})$ is that of Eq. (2) and the first integral is understood to be an improper one. The independent variables will be dropped on the right-hand side for the sake of brevity in the sequel, if no confusion arises.

The second case $\mathbf{x}\to\boldsymbol{\xi}\in\Gamma_h$ is more complex since some of the kernels involved in the limit have higher order singularities. Consider first the integration along Γ. As in the previous case,

$$\int_{\Gamma}\left[u^*\delta q - q^*\delta u\right]\mathrm{d}\Gamma \to (1-c(\boldsymbol{\xi}))\delta u(\boldsymbol{\xi}) + \int_{\Gamma}\left(u^*\delta q - q^*\delta u\right)\mathrm{d}\Gamma \tag{35}$$

when $\mathbf{x}\to\boldsymbol{\xi}\in\Gamma$

Likewise,

$$\int_{\Gamma}\left(u^*\nabla q - q^*\nabla u\right)\cdot\delta\mathbf{y}\,d\Gamma \to (1-c(\boldsymbol{\xi}))\nabla u(\boldsymbol{\xi})\cdot\delta\boldsymbol{\xi} + \int_{\Gamma}\left(u^*\nabla q - q^*\nabla u\right)\cdot\delta\mathbf{y}\,d\Gamma \tag{36}$$

It bears emphasis that the former limits imply that both $\delta u(\mathbf{x})$ and $\nabla u(\mathbf{x})\cdot\delta\mathbf{x}$ are continuous functions at $\boldsymbol{\xi}$, and the same requirements should be fulfilled by the discretized variables.

The limit of the rest of the integrals is carried out by defining a distorted domain as shown in Fig. 3. Consider first,

$$\begin{aligned}&\lim_{\varepsilon\to 0}\int_{\Gamma_h - S_\varepsilon + \Gamma_\varepsilon}\left(\nabla u^* q - \nabla q^* u\right)\cdot(\delta\mathbf{y}-\delta\boldsymbol{\xi})\,\mathrm{d}\Gamma\\ &\quad=\lim_{\varepsilon\to 0}\int_{\Gamma_h - S_\varepsilon}\left(\nabla u^* q - \nabla q^* u\right)\cdot(\delta\mathbf{y}-\delta\boldsymbol{\xi})\,\mathrm{d}\Gamma + \lim_{\varepsilon\to 0}\int_{\Gamma_\varepsilon}\left(\nabla u^* q - \nabla q^* u\right)\cdot(\delta\mathbf{y}-\delta\boldsymbol{\xi})\,\mathrm{d}\Gamma\end{aligned} \tag{37}$$

The integration over the boundary Γ_ε can be handled analytically, regularizing the integrands by series expansion. Taking into account that, $\nabla u^* = -\nabla r/(2\pi r)$ and since $\delta\mathbf{y}-\delta\boldsymbol{\xi}\to 0$ as $\varepsilon\to 0$, then,

$$\lim_{\varepsilon\to 0}\int_{\Gamma_\varepsilon}\nabla u^* q\cdot(\delta\mathbf{y}-\delta\boldsymbol{\xi})\,\mathrm{d}\Gamma = 0 \tag{38}$$

On the other hand, since $\nabla q^* = -(1/2\pi r^2)(\mathbf{n} - 2\nabla r\nabla r\cdot\mathbf{n})$ has a second-order singularity, the following expansion is necessary,

$$u(\mathbf{y})(\delta\mathbf{y}-\delta\boldsymbol{\xi}) = u(\boldsymbol{\xi})\nabla\delta\boldsymbol{\xi}\cdot(\mathbf{y}-\boldsymbol{\xi}) + \text{h.o.t.} \tag{39}$$

to perform the integral of $\nabla q^* u\cdot(\delta\mathbf{y}-\delta\boldsymbol{\xi})$, where $\nabla\delta\boldsymbol{\xi} = \nabla\delta\mathbf{y}(\boldsymbol{\xi})$, and h.o.t. stands for *higher order terms*.

The integral can be regularized as follows,

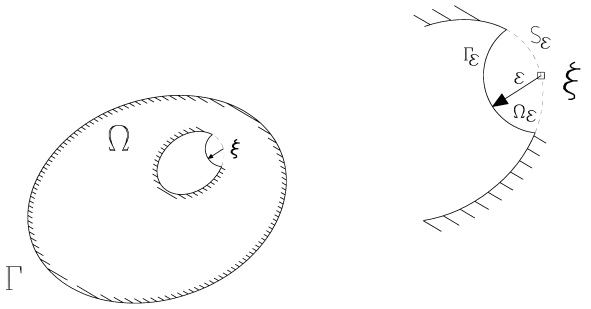

Fig. 3. Modified boundary for the limiting process.

$$\lim_{\varepsilon\to 0}\int_{\Gamma_\varepsilon}\nabla q^*u\cdot(\delta\mathbf{y}-\delta\boldsymbol{\xi})\,\mathrm{d}\Gamma$$

$$=\lim_{\varepsilon\to 0}\int_{\Gamma_\varepsilon}\nabla q^*\cdot\left[u(\delta\mathbf{y}-\delta\boldsymbol{\xi})-u(\boldsymbol{\xi})\nabla\delta\boldsymbol{\xi}\cdot(\mathbf{y}-\boldsymbol{\xi})\right]\mathrm{d}\Gamma+u(\boldsymbol{\xi})\lim_{\varepsilon\to 0}\int_{\Gamma_\varepsilon}\nabla q^*\cdot\nabla\delta\boldsymbol{\xi}\cdot(\mathbf{y}-\boldsymbol{\xi})\,\mathrm{d}\Gamma \tag{40}$$

The first limit on the right-hand side vanishes since the integrand is regular, while the second one can be performed analytically once the shape of Γ_ε is fixed. For the sake of simplicity, an arc of circle is chosen for Γ_ε, although any shape will lead to valid results (see Fig. 4). Thus,

$$\lim_{\varepsilon\to 0}\int_{\Gamma_\varepsilon}\nabla q^*\cdot\nabla\delta\boldsymbol{\xi}\cdot(\mathbf{y}-\boldsymbol{\xi})\,\mathrm{d}\Gamma=\frac{1}{2\pi}\nabla\delta\boldsymbol{\xi}:\int_{\theta_1}^{\theta_2}\langle\mathbf{nn}\rangle\,\mathrm{d}\theta \tag{41}$$

since on the arc $\nabla r=\mathbf{n}$, $(\mathbf{y}-\boldsymbol{\xi})=\varepsilon\mathbf{n}$ and $\mathrm{d}\Gamma=\varepsilon\,\mathrm{d}\theta$;$\langle\mathbf{nn}\rangle$ represents a dyadic product, and the operator ':' stands for the scalar product with respect to both indices, i.e., $\mathbf{a}:\mathbf{b}=a_{ij}b_{ij}$. The remaining integration is easily performed,

$$\boldsymbol{b}'(\xi)=\frac{1}{2\pi}\int_{0_1}^{0_2}\langle\mathbf{nn}\rangle d\theta=\begin{pmatrix}\frac{\theta}{4\pi}+\frac{1}{8\pi}(\sin 2\theta_2-\sin 2\theta_1) & \frac{1}{8\pi}(\cos 2\theta_1-\cos 2\theta_2)\\ \frac{1}{8\pi}(\cos 2\theta_1-\cos 2\theta_2) & \frac{\theta}{4\pi}-\frac{1}{8\pi}(\sin 2\theta_2-\sin 2\theta_1)\end{pmatrix} \tag{42}$$

Summing up,

$$\lim_{\varepsilon\to 0}\int_{\Gamma_h-S_\varepsilon+\Gamma_\varepsilon}\left(\nabla u^*q-\nabla q^*u\right)\cdot(\delta\mathbf{y}-\delta\boldsymbol{\xi})\,\mathrm{d}\Gamma$$

$$=-u(\boldsymbol{\xi})\nabla\delta\boldsymbol{\xi}:\mathbf{b}'(\boldsymbol{\xi})+\int_{\Gamma_h}\left(\nabla u^*q-\nabla q^*u\right)\cdot(\delta\mathbf{y}-\delta\boldsymbol{\xi})\,\mathrm{d}\Gamma \tag{43}$$

where the integral on the right-hand side is understood to be a Cauchy principal value.

A similar approach can be employed to tackle the limit,

$$\lim_{\varepsilon\to 0}\int_{\Gamma_h-S_\varepsilon+\Gamma_\varepsilon}(u^*\nabla u-\nabla u^*u)\cdot\delta\mathbf{m}\,d\Gamma \tag{44}$$

In this limit, only the integral,

$$\lim_{\varepsilon\to 0}\int_{\Gamma_\varepsilon}\nabla u^*u\cdot\delta\mathbf{m}\,d\Gamma \tag{45}$$

leads to a free term. To compute it, the following expansions are used,

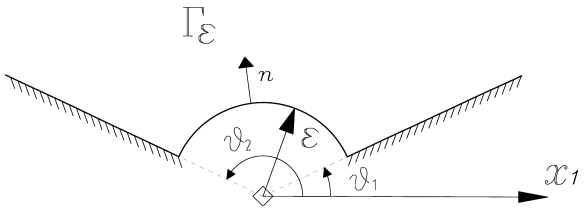

Fig. 4. Circular modified boundary around a singular point.

$$u(\mathbf{y}) = u(\boldsymbol{\xi}) + \text{h.o.t.} \tag{46}$$

$$\delta\mathbf{m} = (\nabla\delta y_2,\ -\nabla\delta y_1)\cdot\mathbf{t} = (\nabla\delta\xi_2,\ -\nabla\delta\xi_1)\cdot\boldsymbol{t} + \text{h.o.t.} \tag{47}$$

where $\mathbf{t}$ is the tangent vector to the boundary.

Since $\nabla u^* = -\mathbf{n}/(2\pi\varepsilon)$ along the arc Γ_ε and $n_1 = t_2, n_2 = -t_1$, the regularization leads to,

$$-\lim_{\varepsilon\to 0}\frac{u(\boldsymbol{\xi})}{2\pi\varepsilon}\int_{\Gamma_\varepsilon}\mathbf{n}\cdot\left[(\nabla\delta\xi_2,\ -\nabla\delta\xi_1)\cdot\boldsymbol{t}\right]\mathrm{d}\Gamma = -u(\boldsymbol{\xi})\nabla\delta\boldsymbol{\xi}:\mathbf{b}(\boldsymbol{\xi}) \tag{48}$$

where

$$\mathbf{b}''(\boldsymbol{\xi}) = \frac{1}{2\pi}\int_{\Gamma_\varepsilon}\langle\boldsymbol{tt}\rangle\,\mathrm{d}\Gamma = \begin{pmatrix} \frac{\theta}{4\pi} - \frac{1}{8\pi}(\sin 2\theta_2 - \sin 2\theta_1) & -\frac{1}{8\pi}(\cos 2\theta_1 - \cos 2\theta_2) \\ -\frac{1}{8\pi}(\cos 2\theta_1 - \cos 2\theta_2) & \frac{\theta}{4\pi} + \frac{1}{8\pi}(\sin 2\theta_2 - \sin 2\theta_1) \end{pmatrix} \tag{49}$$

and therefore,

$$\lim_{\varepsilon\to 0}\int_{\Gamma_h - S_\varepsilon + \Gamma_\varepsilon}(u^*\nabla u - \nabla u^* u)\cdot\delta\mathbf{m}\,d\Gamma = -u(\boldsymbol{\xi})\nabla\delta\boldsymbol{\xi}:\mathbf{b}(\boldsymbol{\xi}) + \int_{\Gamma_h}(u^*\nabla u - \nabla u^* u)\cdot\delta\mathbf{m}\,d\Gamma \tag{50}$$

where the integral on the right-hand side is understood to be a Cauchy principal value, as well.

In summary, the limiting process outlined in this section when $\mathbf{x}\to\boldsymbol{\xi}\in\Gamma_h$ leads to,

$$\begin{aligned} c(\boldsymbol{\xi})\left[\delta u(\boldsymbol{\xi}) + \nabla u(\boldsymbol{\xi})\cdot\delta\boldsymbol{\xi}\right] + \mathbf{b}(\boldsymbol{\xi}):u(\boldsymbol{\xi})\nabla\delta\boldsymbol{\xi} &= \int_\Gamma\left(u^*\delta q - q^*\delta u\right)\mathrm{d}\Gamma - \int_\Gamma\left(\nabla u^* q - \nabla q^* u\right)\cdot\delta\boldsymbol{\xi}\,\mathrm{d}\Gamma \\ &+ \int_{\Gamma_h}\left[\left(\nabla u^* q - \nabla q^* u\right)\cdot\delta\mathbf{y} + \left(u^*\nabla q - q^*\nabla u\right)\cdot\delta\mathbf{y} + (u^*\nabla u - \nabla u^* u)\cdot\delta\mathbf{m}\right]\mathrm{d}\Gamma \end{aligned} \tag{51}$$

which is the Variation BIE for a point $\boldsymbol{\xi}\in\Gamma_h$, where $c(\boldsymbol{\xi}) = \theta/2\pi$ and $\mathbf{b}(\boldsymbol{\xi}) = \mathbf{b}'(\boldsymbol{\xi}) + \mathbf{b}(\boldsymbol{\xi})$. It has to be emphasized that this equation has not been obtained previously to the authors' knowledge.

The Eqs. (34) and (51) are valid for the points on the known boundary Γ_c and the unknown boundary Γ_h, respectively. In fact, Eq. (51) comprises Eq. (34) since substituting $\delta\boldsymbol{\xi} = 0$ in the first one leads to the second one. Therefore, Eq. (51) is the *Variation Boundary Integral Equation* (δBIE) for any point $\boldsymbol{\xi}\in\Gamma$.

4.1. Boundary conditions for the inverse problem

The δBIE in Eq. (51) has to be completed with a set of boundary conditions for δu and δq. These boundary conditions for the inverse problem can be obtained by expanding the boundary conditions of the primary problem with respect to the variations of the geometry, and linearizing the resulting expression.

Four cases have to be distinguished depending on which are the boundary conditions for the primary problem: known potential on Γ_c, known flux on Γ_c, known potential on Γ_h and known flux on Γ_h. Actually, the last two cases encompass the first two, and therefore, only those are outlined.

4.1.1. Known potential on Γ_h

In the primary problem, both in the actual and assumed configuration, the boundary conditions are:

$$u(\tilde{\mathbf{y}}, \tilde{\Gamma}_h) = \bar{u} \tag{52}$$

$$u(\mathbf{y}, \Gamma_h) = \bar{u} \tag{53}$$

Expanding the difference of these conditions $u(\tilde{\mathbf{y}}, \tilde{\Gamma}_h) - u(\mathbf{y}, \Gamma_h) = 0$ we obtain, $\delta u(\mathbf{y}) + \nabla u(\mathbf{y}) \cdot \delta \mathbf{y} = 0$ and therefore,

$$\delta u(\mathbf{y}) = -\nabla u(\mathbf{y}) \cdot \delta \mathbf{y} \tag{54}$$

4.1.2. Known flux on Γ_h

In the primary problem, the boundary conditions are:

$$q(\tilde{\mathbf{y}}, \tilde{\Gamma}_h) = \bar{q} \tag{55}$$

$$q(\mathbf{y}, \Gamma_h) = \bar{q} \tag{56}$$

Recalling Eq. (27) and the definition of δq in Eq. (6), the following equation is obtained,

$$\delta q(\mathbf{y}) = -\nabla(\mathbf{y}, \Gamma_h) \cdot \delta \mathbf{y} - \nabla u(\mathbf{y}, \Gamma_h) \delta \mathbf{n}(\mathbf{y}) \tag{57}$$

When $\bar{q} = 0$, this expression can be rewritten as,

$$\delta q(\mathbf{y}) = -\nabla q(\mathbf{y}, \Gamma_h) \cdot \delta \mathbf{y} - \nabla u(\mathbf{y}, \Gamma_h) \delta \mathbf{m}(\mathbf{y}) \tag{58}$$

since $\nabla u(\mathbf{y}, \Gamma_h) \delta \mathbf{n}(\mathbf{y}) = \nabla u(\mathbf{y}, \Gamma_h) \delta \mathbf{m}(\mathbf{y}) - \bar{q}(\mathbf{y}, \Gamma_h) \delta J = \nabla u(\mathbf{y}, \Gamma_h) \delta \mathbf{m}(\mathbf{y})$

The boundary conditions for the inverse problem when the primary boundary conditions are known potential or flux on Γ_c, are simply $\delta u = 0$ and $\delta q = 0$, respectively.

5. Boundary element discretization and solution method

In this section, the numerical solution of the set of integral equations comprised of the BIE of the *direct* problem (Eq. (2)) and the δBIE of the *inverse* problem (Eq. (51)) is presented. The discretization is dealt with in depth in Gallego and Suarez (1999), and therefore, it will be just outlined here.

The numerical solution of the δBIE is performed by the boundary element method. Standard boundary elements can be used to interpolate the variations of potential (δu), flux (δq) and geometry ($\delta \mathbf{y}$) in the δBIE. However, due to the continuity requirement established in the previous section, the collocation points cannot be set at the element ends (see Gallego and Domínguez, 1996, for an application of this idea to fracture dynamics problems).

The discretization of the primary BIE leads to the well known set of algebraical equations,

$$\mathbf{Hu} = \mathbf{Gq} \tag{59}$$

where the vectors $\mathbf{u} = (u^1, u^2, \ldots, u^N)$ and $\mathbf{q} = (q^1, q^2, \ldots, q^N)$ collect the potential and flux at the interpolation nodes. After the application of the primary boundary conditions to the former set, a square system of equations is obtained whose solution completely determined the vectors $\mathbf{u}$ and $\mathbf{q}$.

On the other hand, the discretization of the inverse δBIE leads to the following set of equations,

$$\mathbf{H}\delta\mathbf{u} = \mathbf{G}\delta\mathbf{q} + \mathbf{\Delta dx} \tag{60}$$

where the vectors $\delta\mathbf{u}$ and $\delta\mathbf{q}$ collect the variations of the potential and the flux at the interpolation nodes, respectively. The variation of the geometry of the boundary Γ_h is in the vector $\delta\mathbf{x} = (\delta\mathbf{x}^1, \delta\mathbf{x}^2, \ldots, \delta\mathbf{x}^N)$. The matrix $\mathbf{\Delta}$ depends on the kernels u^* and q^*, and the potentials and fluxes at the nodes computed in the direct problem. The application of the inverse boundary conditions yields,

$$\mathbf{H}_R\delta\mathbf{v} = \tilde{\mathbf{\Delta}}\delta\mathbf{x} \tag{61}$$

where $\delta\mathbf{v}$ are the N unknown variations of the potential and/or fluxes. The right-hand side matrix $\tilde{\mathbf{\Delta}}$ proceeds form $\mathbf{\Delta}$ and the boundary conditions.

The former set of N equations cannot be solved since the number of unknowns is $N + 2N_h$, where N_h is the number of interpolation nodes on the boundary $\tilde{\Gamma}_h$. To solve it, the M experimental values are taken into account. At the points on Γ_c where the potential is measured, $\delta u = u(\mathbf{y}, \tilde{\Gamma}_h) - u(\mathbf{y}, \Gamma_h)$ can be computed since $u(\mathbf{y}, \Gamma_h)$ is known from the primary problem. Likewise at the points where the flux is measured, δq can be computed. The number of unknowns is, therefore, reduced to $N + 2N_h - M$. A further reduction is necessary and this can be done by parameterizing the variation of the geometry,

$$\delta\mathbf{x} = \mathbf{P}\delta\mathbf{g} \tag{62}$$

The vector $\delta\mathbf{g}$ has only six components which are: the variation of the center of the flaw (δx_c, δy_c), the variation of the rotation of the flaw (δw), and the variation of the deformation of the flaw ($\delta\varepsilon_{xx}$, $\delta\varepsilon_{yy}$, $\delta\varepsilon_{xy}$). It bears emphasis that it is the variation of the geometry of the flaw what is parameterized and not the geometry of the flaw. A clear advantage of this approach is that this parameterized variation can be applied to any shape for the assumed flaw. The assumed flaw is translated, rotated and distorted by application of the transformation $\mathbf{x} \rightarrow \mathbf{x} + \delta\mathbf{x} = \mathbf{x} + P\delta\mathbf{g}$.

This idea can be extended by applying a linear, quadratic, ..., field of distortion to the flaw, increasing in, therefore, the number of geometrical parameters which define the aforementioned transformation (Gallego and Suarez, 1999).

Substituting Eq. (62) in Eq. (61) and collecting the unknowns to the left-hand side gives a non-square system of equations

$$\mathbf{A}\delta\mathbf{h} = \mathbf{b} \tag{63}$$

The number of equations is N and the number of unknowns $N - M + 6$. Obviously, $M \geq 6$, i.e. the number of experimental measurements should be greater than or equal to the number of geometrical parameters, in order to obtain a square or overdetermined system of equations.

The solution of this overdetermined system of equations can be tackle by the *weighted least squares* method, which leads to the system,

$$\mathbf{A}^T\mathbf{W}\mathbf{A}\delta\mathbf{h} = \mathbf{A}^T\mathbf{W}\mathbf{b} \tag{64}$$

where $\mathbf{W} = \mathrm{diag}(w_1, w_2, \ldots, w_N)$ collects the set of weighting factors. In all the application solved, the weights have been set to 1, but it is postulated that bigger weights in the equations corresponding to points where the experimental measures are taken, would lead to an improvement in the convergence of the method.

The solution of this system of equations yields the unknown geometrical parameters $\delta\mathbf{g}$. By using Eq. (62), $\delta\mathbf{x}$ is computed and the flaw shape updated. The procedure is repeated after convergence is attained.

6. Numerical results

Four sets of numerical applications are presented in this section in order to asses the performance of the proposed approach. The first two examples have been taken from the paper by Mitra and Das (1992) for the sake of comparison. In this paper the authors minimize a functional by the Levengerg–Marquadt algorithm assuming an elliptical shape for the flaw. The solution is further improved in a second stage using a B-spline representation for the flaw, although this refined results will not be considered in the comparisons hereinafter. The last two applications are more challenging since simulated experimental errors are included in the first, and two flaws are considered in the second one. With these applications, the performance and range of validity of the method are demonstrated.

6.1. Centered elliptical flaw

The actual flaw is an ellipse whose semi-axes are $a = 0.05$ and $b = 0.025$. The ellipse is at the center of a 2×2 square and its major axis lies along the x-axis. The boundary conditions and the geometry are shown in Fig. 5. The assumed flaw is a circle around the actual flaw of radius 0.1. The problem has been solved with different number of experimental measurements, $M = 8$, 10 and 12 and a discretization of the flaw with eight quadratic elements and the exterior boundary with 16 quadratic elements, four per side. The experimental data have been simulated simply by solving the direct problem with a direct BE code. Some of the results are shown in Table 1 (node 1 is the lower right corner and has coordinates (2,0)). For the first case ($M = 8$), we took as experimental data the flux in nodes 4, 8, 19 and 22, and the potential in nodes 12, 16, 27 and 31. For the second case ($M = 10$), we added the flux in node 5 and the potential in node 29. Finally, for the third case ($M = 12$), we included the potential in node 14 and the flux in node 20.

The number of iterations needed to attain the convergence and the final values of the semi-axis a and b are shown in Table 2. For the sake of comparison, it bears emphasis that the number of iterations to solve the same problem by the algorithm proposed by Mitra ranges from 81 to 83 depending on the number of experimental measurements. The present procedure converges much faster than the approach of Mitra, although the final configuration is not as close as with their algorithm. It should be noted that the present approach do not minimize any residual at all, and therefore, when the assumed flaw and the actual flaw are close enough, the resulting potential and fluxes on the boundary are very similar, and therefore, the "driving force" which "moves" the flaw almost vanishes. In Fig. 6, the shapes of the

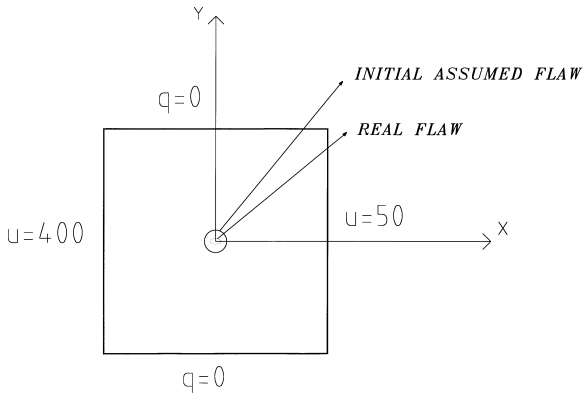

Fig. 5. Centered elliptical flaw: geometry, boundary conditions, actual and initial configuration.

Table 1
Simulated experimental data for the centered elliptical flaw (q flux, u potential)

Node	Coordinates	Data
4	(2.00, 0.75)	(q) −174.64
5	(2.00, 1.00)	(q) −174.58
8	(2.00, 1.75)	(q) −174.84
12	(1.25, 2.00)	(u) 181.22
14	(0.75, 2.00)	(u) 268.78
16	(0.25, 2.00)	(u) 356.28
19	(0.00, 1.50)	(q) 174.76
20	(0.00, 1.25)	(q) 174.64
22	(0.00, 0.75)	(q) 174.64
27	(0.50, 0.00)	(u) 312.54
29	(1.00, 0.00)	(u) 225.00
31	(1.50, 0.00)	(u) 137.46

initial, final and intermediate iterations are shown for the case of 12 experimental measurements. It can be seen that the actual and the computed flaws are practically indistinguishable.

6.2. L-shape flaw

In this example, the flaw is an L-shape crack as shown in Fig. 7. The flaw is 0.1 units wide and its arms are 0.3 units long. The geometry of the exterior boundary, the boundary conditions, the initial assumed flaw and BE model are as in the foregoing example. The $M = 20$ simulated experimental data have been used (see Table 3).

The final and intermediate configurations of the flaw are shown in Fig. 8. The convergence is attained in only eight iterations, while the procedure by Mitra et al. needs 29 iterations to arrive at the same configuration.

6.3. L-shape flaw: simulated experimental errors

In these series of examples, the geometry of the exterior boundary, the shape and position of the real flaw and the boundary conditions are as in the foregoing example. The initial assumed flaw now has the same form as the real one, but it is displaced from its position, as shown in Fig. 9. For the BE model, 10 elements have been used for the assumed flaw and eight for the exterior boundary. Five set of experimental measures have been simulated. The first set has been generated as in the previous examples, solving the problem by a direct BE code. The rest of the sets have been generated from this one adding a random error to each measure with the values $\pm 1\%$, $\pm 2\%$, $\pm 3\%$, $\pm 5\%$, respectively. In Table 4, the five sets are listed.

Table 2
Results for the centered elliptical flaw

M	Iteration No.	a	b
8	4	0.0275	0.0318
10	5	0.0433	0.0267
12	5	0.0471	0.0258

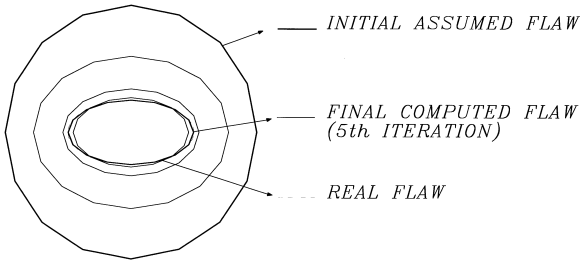

Fig. 6. Centered elliptical flaw: intermediate and final computed flaw.

The final and intermediate configurations of the flaw are shown in Figs. 10–14 for each case. It can be seen that the smaller the simulated errors, the closer the final computed flaw to the real one, as can be expected. For the simulated error $\pm 5\%$, the final configuration is very far from the real one. However, consider Fig. 15 where the evolution of the residual function,

$$F(\Gamma_h) = \sum_{i=1}^{M} \left(x_i^{\mathrm{ex}} - x_i\right)^2 \tag{65}$$

is shown. In this definition, x^{ex} represents an experimentally known quantity (potential or flux) and x_i its computed value for a given position of the assumed cavity. It can be seen that the residual function evolves until it attains a stable value, although the position of the flaw is not close to the "real" one. Taking into account that given the magnitude of the error (5% in each measure), the set of experimental measures is very far from the exact values of the boundary variables. In fact, the residual of this set of errors with respect to the exact ones is about 860, and therefore, as shown in Fig. 15, the final value of the residual is of the same order as it can be expected. It is possible that other position of the flaw closer to the real one could produce a similar or smaller residual, but the procedure is unable to find it since there is a local minimum of the residual function around the finally attained position.

6.4. Two real flaws

The exterior boundary is again a 2×2 square with flux and potential conditions as in the first

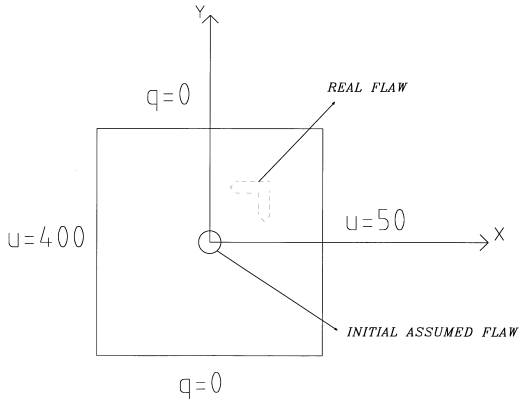

Fig. 7. L-shape flaw: geometry, boundary conditions, actual and initial configuration.

Table 3
Simulated experimental data for the L-shape flaw (q flux, u potential)

Node	Coordinates	Data
2	(2.00, 0.25)	(q) −179.90
3	(2.00, 0.50)	(q) −180.04
5	(2.00, 1.00)	(q) −171.12
7	(2.00, 1.50)	(q) −145.96
8	(2.00, 1.75)	(q) −160.86
10	(1.75, 2.00)	(u) 92.40
11	(1.50, 2.00)	(u) 137.53
12	(1.25, 2.00)	(u) 184.94
14	(0.75, 2.00)	(u) 274.48
16	(0.25, 2.00)	(u) 358.40
18	(0.00, 1.75)	(q) 166.19
19	(0.00, 1.50)	(q) 166.00
20	(0.00, 1.25)	(q) 166.22
22	(0.00, 0.75)	(q) 168.22
24	(0.00, 0.50)	(q) 170.11
26	(0.25, 0.00)	(u) 357.38
27	(0.50, 0.00)	(u) 314.62
28	(0.75, 0.00)	(u) 271.57
30	(1.25, 0.00)	(u) 184.12
32	(1.75, 0.00)	(u) 94.90

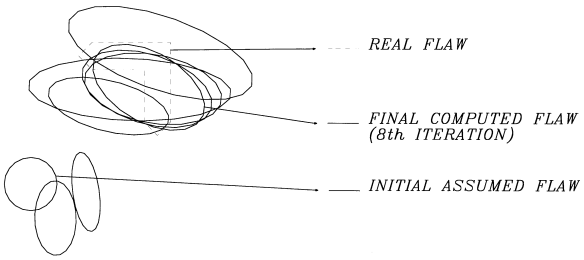

Fig. 8. L-shape flaw: intermediate and final computed flaw.

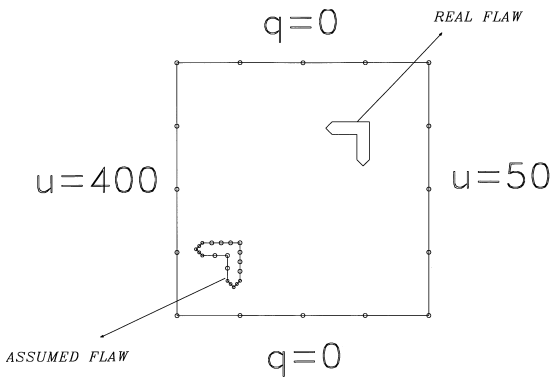

Fig. 9. L-shape flaw: geometry, boundary conditions, actual and initial configuration, for the problem with simulated experimental errors.

Table 4
Simulated experimental data for the L-shape flaw with random errors (q flux, u potential)

Node	Coordinates	Exact data	Data ±1%	Data ±2%	Data ±3%	Data ±5%
6	(1.50, 2.00)	(u) 137.72	136.34	134.96	133.58	130.83
7	(1.00, 2.00)	(u) 231.10	228.79	226.48	224.17	219.54
8	(0.50, 2.00)	(u) 316.76	319.93	323.09	326.26	332.60
14	(0.50, 0.00)	(u) 314.67	317.82	320.96	324.11	330.40
15	(1.00, 0.00)	(u) 228.16	225.88	223.59	221.31	216.75
16	(1.50, 0.00)	(u) 139.70	141.10	142.50	143.90	146.69

example. The real defect is composed now by two flaws as shown in Fig. 16. The initially assumed flaw (a centered circle), and the BE model are shown in this figure as well. $M = 20$ experimental values computed by a direct BE code are provided for the identification of the flaws (see Table 5).

The computed intermediate and final shape and position of the flaw are shown in Fig. 17. The proposed procedure converges to a final flaw which is close to the real flaws in 20 iterations. The residual decreases from its initial value, 78.39–0.50 which is almost negligible, taking into account the magnitude of the variables and that the exact value is unattainable.

7. Conclusions

A new approach to solve inverse problem by the Boundary Element Method is presented in this paper. The approach is well-suited for the so-called identification inverse problem where part of the boundary of a domain is unknown beforehand, and has to be estimated using additional experimental data. Since these data usually pertains to boundary points, the use of Boundary Integral Equations

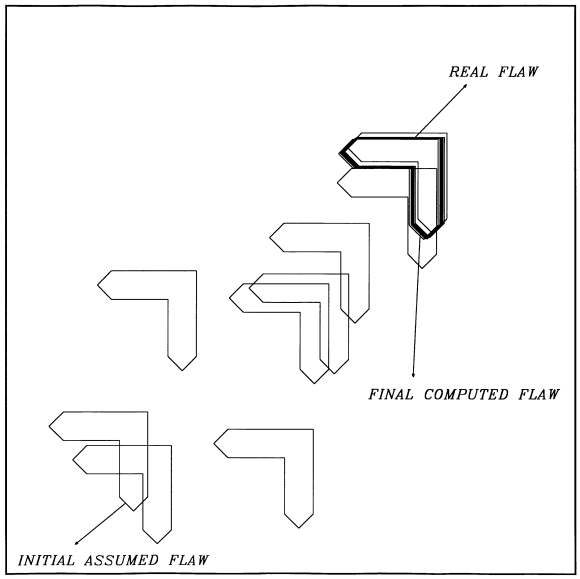

Fig. 10. L-shape flaw: intermediate and final computed flaw (experimental error 0%).

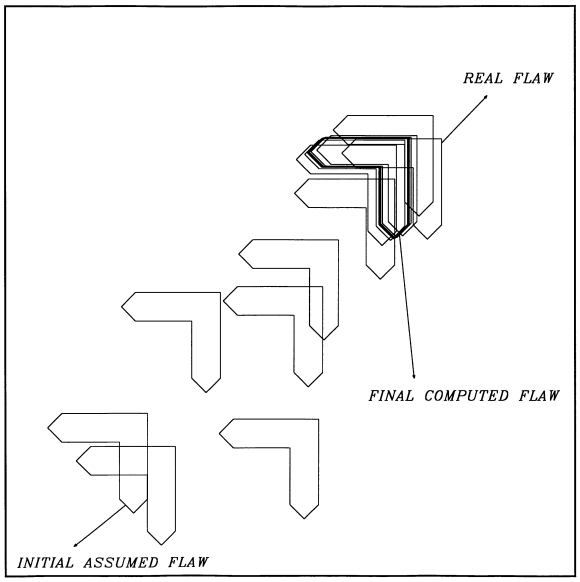

Fig. 11. L-shape flaw: intermediate and final computed flaw (experimental error 1%).

seems particularly attractive. In this paper, the Variation Boundary Integral Equation is deduced. This equation is first computed for an interior point and then, through a limiting process, is carried to both the known and the unknown part of the boundary. This approach is very convenient since the derivation of the δBIE for an interior point has no difficulties associated to the presence of singular integral, and the ensuing limit to the boundary can be carried out using techniques already developed

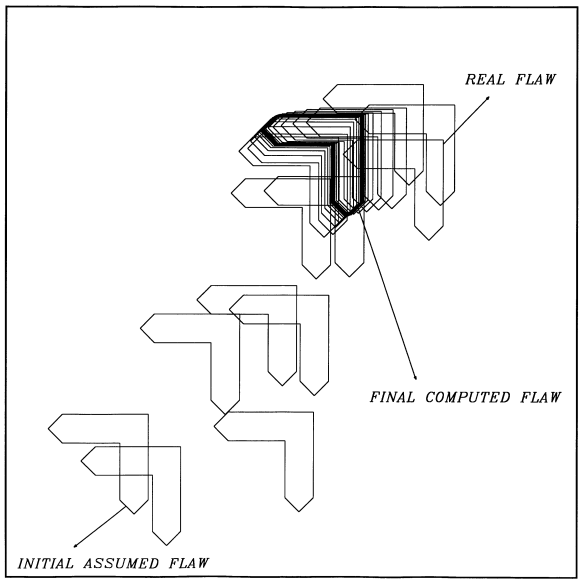

Fig. 12. L-shape flaw: intermediate and final computed flaw (experimental error 2%).

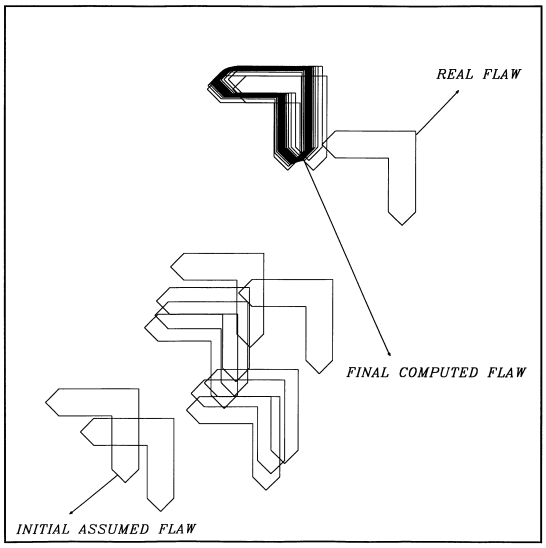

Fig. 13. L-shape flaw: intermediate and final computed flaw (experimental error 3%).

for other Boundary Integral Equations. In this work, a complete derivation of the δBIE is provided, improving previous attempts (Zeng and Saigal, 1992; Tanaka and Masuda, 1989) where some terms were lacking. The δBIE can be discretized using advanced Boundary Element techniques giving rise to a set of algebraic equations. These equations are solved using the least squares method since the number of unknowns is less than the number of equations, provided that the number of experimental measurements is bigger than the number of parameters which defined the variation of the flaw. Several

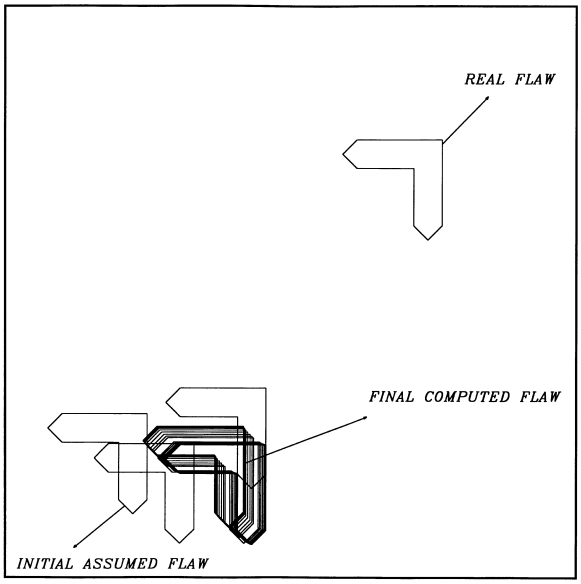

Fig. 14. L-shape flaw: intermediate and final computed flaw (experimental error 5%).

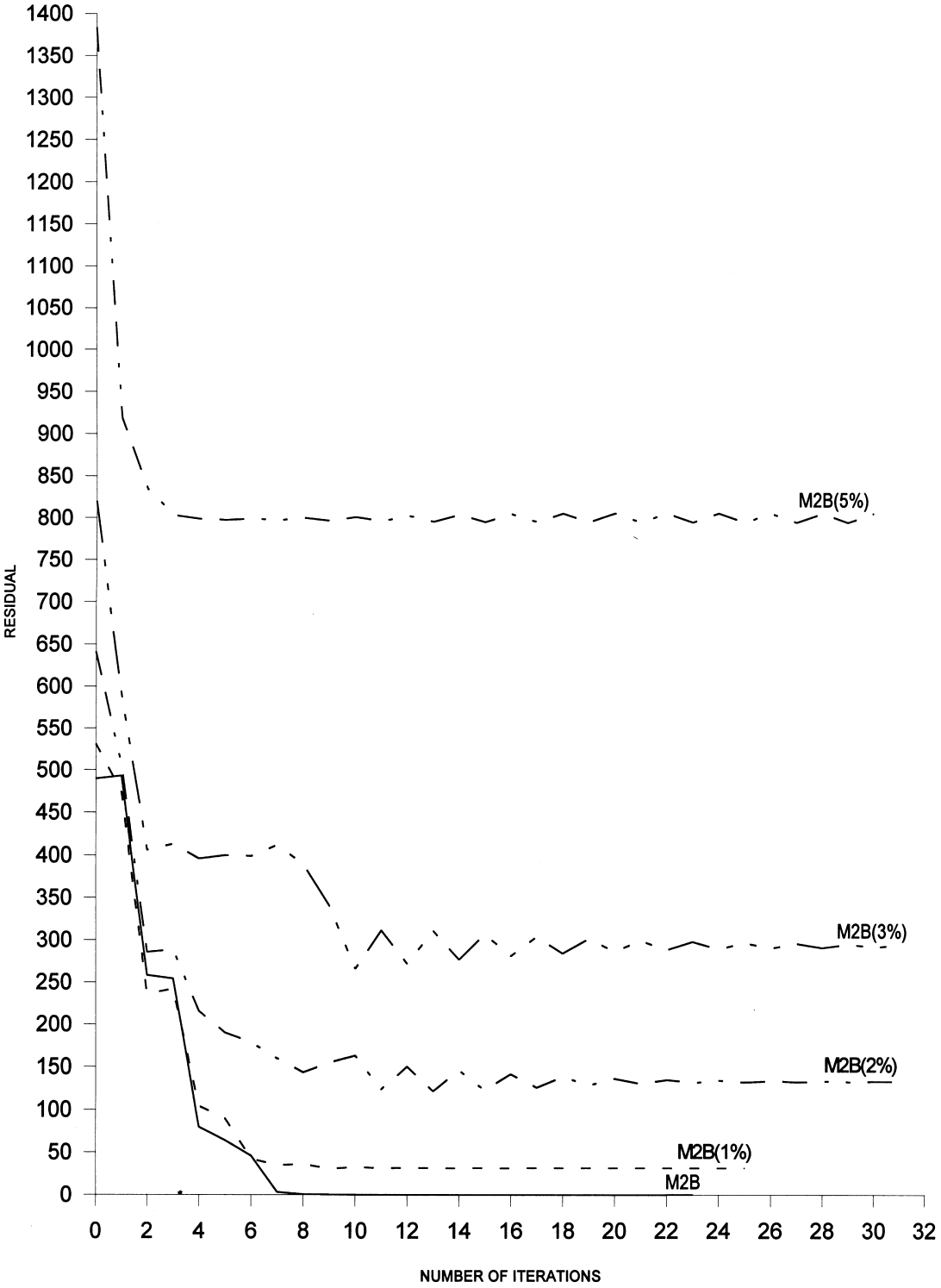

Fig. 15. L-shape flaw: evolution of the residual for different simulated errors.

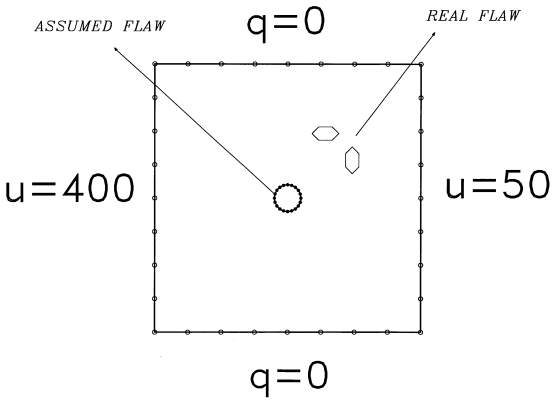

Fig. 16. Two real flaws: geometry, boundary conditions, actual and initial configuration.

examples are presented which asses the performance of the method under severe testing conditions, including experimental error in the data and existence of a number of flaws different from the assumed. A drawback of the proposed approach is the need of solving two systems of equations in every iteration step. Only if the number of iteration is at least halved with respect to alternative approaches, this extra cost would be justify. Nevertheless, a more efficient approach to solve the system of Eq. (63) is under development, which leads to a much smaller overdetermined system of equations with the number of unknowns equal to the number of experimental measures.

Table 5
Simulated experimental data for the problem with two flaws (q flux, u potential)

Node	Coordinates	Data
2	(2.00, 0.25)	(q) −176.42
3	(2.00, 0.50)	(q) −176.22
5	(2.00, 1.00)	(q) −171.16
7	(2.00, 1.50)	(q) −166.81
8	(2.00, 1.75)	(q) −171.95
10	(1.75, 2.00)	(u) 93.59
11	(1.50, 2.00)	(u) 137.94
12	(1.25, 2.00)	(u) 183.09
14	(0.75, 2.00)	(u) 271.31
16	(0.25, 2.00)	(u) 357.17
18	(0.00, 1.75)	(q) 171.26
19	(0.00, 1.50)	(q) 171.29
20	(0.00, 1.25)	(q) 171.52
22	(0.00, 0.75)	(q) 172.51
24	(0.00, 0.50)	(q) 173.30
26	(0.25, 0.00)	(u) 356.64
27	(0.50, 0.00)	(u) 313.22
28	(0.75, 0.00)	(u) 269.70
30	(1.25, 0.00)	(u) 182.17
32	(1.75, 0.00)	(u) 94.10

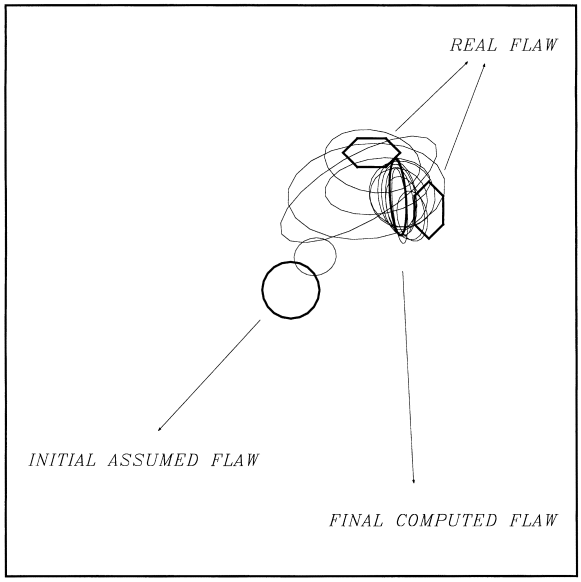

Fig. 17. Two real flaws: intermediate and final computed flaw.

Acknowledgements

This work was supported by the Dirección General de Enseñanza Superior of Spain under the Research Project No. PB96-1409.

References

Bonnet, M., 1995. BIE and material differentiation applied to the formulation of obstacle inverse problems. Engrg. Anal. Boundary Elements 15, 121–136.

Bui, H.D., 1994. Inverse Problems in the Mechanics of Materials: An Introduction. CRC Press, Boca Raton.

Brebbia, C.A., Dominguez, J., 1978. Boundary Elements: An Introductory Course. Computational Mechanics Publications, Southampton.

Gallego, R., Suarez, J., 1999. Numerical solution of a new variation boundary integral equation for inverse problems. Int. J. Numer. Methods Engrg, in press.

Gallego, R., Domínguez, J., 1996. Hypersingular BEM for transient elastodynamics. Int. J. Numer. Methods Engrg 39 (10), 1681–1705.

Guiggiani, M., 1992. Direct evaluation of hypersingular integrals in 2D BEM. In: Hackbusch, W. (Ed.), Notes on Numerical Fluid Mechanics, vol. 33. Vieweg, Braunschweig, pp. 23–34.

Mitra, A.K., Das, S., 1992. Solution of inverse problem by using the boundary element method, Boundary Element Technology XVII. Computational Mechanics Publications, Southampton, pp. 721–731.

Mellings, S.C., Aliabadi, M.H., 1993. Dual boundary element formulation for inverse potential problems in crack identification. Engrg. Anal. Boundary Elements 12, 275–281.

Nishimura, N., Kobayashi, S., 1991. A boundary integral equation method for an inverse problem related to crack detection. Int. J. Numer. Methods Engrg 32, 1371–1387.

Nishimura, N., Kobayashi, S., 1994. Determination of cracks having arbitrary shapes with the boundary integral equation method. Engrg. Anal. Boundary Elements 15, 189–195.

Nishimura, N., 1997. Cracks determination problems. In: Yagawa, G., Miki, C. (Eds.), Theoretical and Applied Mechanics, vol. 46, pp. 39–57.

Tanaka, M., Masuda, Y., 1989. Boundary element method applied to some inverse problems. Engineering Analysis 3 (3), 138–143.

Zeng, X., Saigal, S., 1992. An inverse formulation with boundary elements. Journal of Applied Mechanics 59, 835–840.